

Adsorption of phosphates from water by two polymer-silicate composites

Kalpani E. H. Wijesinghe , Rasika E. A. Dissanayake , Sithy S. Iqbal , Namal Priyantha & Mohamed C. M. Iqbal

To cite this article: Kalpani E. H. Wijesinghe , Rasika E. A. Dissanayake , Sithy S. Iqbal , Namal Priyantha & Mohamed C. M. Iqbal (2020): Adsorption of phosphates from water by two polymer-silicate composites, Bioremediation Journal, DOI: [10.1080/10889868.2020.1811631](https://doi.org/10.1080/10889868.2020.1811631)

To link to this article: <https://doi.org/10.1080/10889868.2020.1811631>



View supplementary material [↗](#)



Published online: 27 Aug 2020.






Submit your article to this journal [↗](#)



View related articles [↗](#)



Adsorption of phosphates from water by two polymer-silicate composites

Kalpani E. H. Wijesinghe^{a,b}, Rasika E. A. Dissanayake^a , Sithy S. Iqbal^c , Namal Priyantha^d, and Mohamed C. M. Iqbal^a 

^aPlant and Environmental Sciences, National Institute of Fundamental Studies, Kandy, Sri Lanka; ^bPostgraduate Institute of Science, University of Peradeniya, Peradeniya, Sri Lanka; ^cDepartment of Chemistry, Faculty of Natural Sciences, Open University of Sri Lanka, Nawala, Sri Lanka; ^dDepartment of Chemistry, Faculty of Science, University of Peradeniya, Peradeniya, Sri Lanka

ABSTRACT

Phosphorus is an essential plant nutrient required by all living organisms and global phosphate resources, being finite, are expected to last another 125 years. This study investigated a sustainable approach to retrieving phosphates from aqueous media using a composite of commonly available biological and mineral sources. Two composites were synthesized using (i) feldspar, alginate, and agar cross-linked by ferric and calcium ions (FAA), and (ii) feldspar, fly ash, and alginate crosslinked with copper ions (FFA). Adsorption parameters were determined using a synthetic phosphate solution. The FAA composite adsorbed 69% of the phosphates within 4 hours; 81% was adsorbed after equilibrium was reached in 9.5 h (pH 4–10). The FFA composite adsorbed 82% of the phosphate reaching equilibrium after 5.5 h (pH 3–7). Characterization of the composite by scanning electron microscopy and Fourier Transform Infrared spectroscopy showed the presence of inorganic and organic functional groups in the agar and alginate that could adsorb phosphate ions. The kinetic and isotherm data suggest that the phosphate ions migrate to the composite boundary and are precipitated by the Ca^{2+} , Fe^{3+} , and Cu^{2+} in the composite matrix. Once the outer composite is saturated, the rest of the phosphate ions are entrapped by the biopolymers through H and covalent bonding. These two biopolymer composites can be easily synthesized and scaled up for phosphate adsorption. Recovery of the adsorbed phosphates, in future studies, can be used for plant nutrition to complete the open-ended cycle of phosphates leaching into water bodies.

KEYWORDS


Adsorption; eutrophication; feldspar-alginate composites; isotherm; kinetic; phosphates


Introduction

All life forms require phosphorus for their cellular metabolism and as an indispensable component of DNA and RNA it is an essential nutrient for all living beings. The excess use of phosphate fertilizers in agriculture leaches downstream and is concentrated in lakes, tanks, and other surface water bodies. Wastewater from industries such as water-based paints, plastics, and cleaning solutions also contribute to high levels of phosphate in surface water. The increase in phosphate along with nitrogen in water bodies causes the environmental issue of eutrophication resulting in uncontrolled growth of aquatic plants, algae, and cyanobacteria (Yoon et al. 2018). This increases the biological oxygen demand (BOD) in water affecting aquatic life. Algal blooms are common

in such water bodies restricting photosynthesis of aquatic plants and reduction in the transparency of water. The phosphate concentration, in water bodies, should be maintained between 0.01 and 0.02 mg L⁻¹ to avoid the consequences of eutrophication (Daniel, Sharpley, and Lemunyon 1998).

Phosphate is a finite resource without alternatives. At the present rates of consumption, global reserves should last for another 125 years (Gilbert 2009). This, however, includes offshore reserves and those with high levels of impurities such as cadmium. Producing usable phosphate from these reserves has a cost on the environment and the economy. If this is excluded, the remaining reserves of clean phosphate rock would last only another 50 years (Gilbert 2009; Rosemarin 2004).

CONTACT Sithy S. Iqbal  ssiqb@ou.ac.lk  Department of Chemistry, Faculty of Natural Sciences, Open University of Sri Lanka, Nawala, Sri Lanka.

 Supplemental data for this article can be accessed at <https://doi.org/10.1080/10889868.2020.1811631>.

© 2020 Taylor & Francis Group, LLC

These estimates come with some caveats: reliable data is unavailable on the global supply and the increase in population will require increased food production.

Methods available to remove phosphate from wastewater include chemical treatment (Caravelli, Contreras, and Zaritzky 2010), enhanced biological phosphorus removal by polyphosphate accumulating organisms (Caravelli, Contreras, and Zaritzky 2010; Oehmen et al. 2007), and adsorption processes (Yoon et al. 2018; Liu et al. 2020; Jang and Lee 2019). The synthetic adsorbent, $\text{Fe}(\text{OH})_3$, has a 100% adsorption efficiency for phosphate and a maximum adsorption capacity of 65 mg/g (Yoon et al. 2018). A lanthanum-chitosan adsorbent was reported with maximum adsorption capacity of 31.01 mg g^{-1} at pH 6 (Liu et al. 2020). Jang and Lee (2019) developed chitosan/Ca-organically modified montmorillonite beads for phosphate adsorption and it show high affinity for phosphate. He et al. (2020) prepared a Ce(III) nanocomposite by partial thermal decomposition of Ce-MOF. Even though this composite has a high phosphate adsorption capacity, the synthesis of the composite requires high temperatures of 400 °C and 500 °C. It is also necessary that the adsorbed phosphorus is in an available form so that the phosphorus-loaded adsorbents are useful as agriculture fertilizers. Biochar derived from sugar beet tailings showed a phosphate removal efficiency of 73% from an aqueous solution of potassium phosphate (Yao et al. 2011). This would ensure that the open-ended phosphorus cycle is closed to recycle the globally depleting phosphorus. Of the methods available, the adsorption process is environmentally friendly, economical, requires minimum labor and in most cases, the end products are not harmful and biodegradable. They are also effective at low concentrations of phosphates.

In this study two novel composites synthesized from organic materials (agar and alginate), and inert inorganic materials (feldspar and fly ash) were used to remove phosphates from the aqueous environment. The emphasis was to use commonly available natural material, which can be returned to the soil with the adsorbed phosphates. Agar is a polysaccharide obtained from algae (phylum Rhodophyta) (Duckworth and

Yaphe 1971). The basic alternating repeating sequences are 1,3-linked β -D-galactopyranose and 1,4-linked 3,6-anhydro- α -L-galactopyranose (Lahaye and Rochas 1991a). Agar is soluble in hot water ($>60^\circ\text{C}$) and solidifies on cooling (Lahaye and Rochas 1991a). Functional groups, such as SO_3^- , COOH , and OH are present in agar.

Alginate is a biopolymer abundantly found in brown algae or Phaeophyceae such as *Laminaria hyperborean*, *Laminaria digitata*, and *Ascophyllum nodosum* (Chan, Jin, and Heng 2002; Lee and Mooney 2012). It is an anionic polymer dissolving in hot water ($>80^\circ\text{C}$) and gelatinized by cross-linking with cations, such as Ca^{2+} , Cu^{2+} , Fe^{2+} , and Fe^{3+} (Lee and Mooney 2012). Alginic acid has been used for water purification by removal of cations such as Cu^{2+} , Cd^{2+} , Zn^{2+} (Lu and Wilkins 1996), and many more. A cellulose-based polymeric material has been used as an adsorbent for the removal of phosphate from aqueous solutions (Luengo et al. 2006). Feldspar is an aluminosilicate ($\text{Al}_2\text{Si}_2\text{O}_8$) that belongs to the group of tectosilicates with the presence of $\text{NaAlSi}_3\text{O}_8$, $\text{CaAl}_2\text{Si}_2\text{O}_8$, or KAlSi_3O_8 (Parsons 2012).

This paper describes a novel approach to adsorb phosphates from water by a cross-linked composite prepared using feldspar, agar and alginate (FAA) and feldspar, fly ash and alginate (FFA). These three components were used for their distinctive properties. Feldspar gives the rigid core to the composite while the biomaterials agar and alginate provide the functional groups for phosphate adsorption.

Materials and methods

Analytical methods

The concentration of aqueous phosphate was determined using UV-Visible spectrophotometer (Analytik Jena, Specord 210 plus, Germany) by the ascorbic acid blue method (Murphy and Riley 1962) at 880 nm wavelength. All the suspensions were agitated on a linear shaker (Wiseshake SHR-2D, Korea). The pH of phosphate solutions was measured using a benchtop pH meter (Orion 2 star, Singapore). The scanning electron

microscope images were obtained from Zeiss Evo ls15 (Carl Zeiss Microscopy, United States). Fourier Transform Infrared (FT-IR) spectra of the composites were obtained using FTIR spectrophotometer (Thermosience model Nicolet 6700, United States). To determine the surface charge of the composites, potentiometric titrations were conducted as described by Chathuranga et al. (2013) using an 848 Titrino plus potentiometric autotitrator (Metrohm, Switzerland). All the experiments were carried out at room temperature.

Composite preparation

A suspension of agar (Fisher Scientific, United Kingdom) and feldspar (from Matale, Sri Lanka) in 1:2 ratio (w/w) was prepared in distilled water. Thereafter, 2.5 g of alginate (Sisco Research Laboratories, India) was dissolved in 100 mL of distilled water maintained at 80 °C, the solution added to the agar/feldspar suspension, and the mixture stirred for 6 h. To cross-link the feldspar-alginate-agar mixture, a solution containing 3% CaSO₄ (BDH Chemicals, England) and 0.5% Fe₂(SO₄)₃ (May and Baker Ltd. Dagenham, England) (w/v) was used. The feldspar-agar-alginate mixture was added to the above solution using a 50 mL disposable syringe (Changzhou medical appliances, China) through a 200 µm pipette tip. The resulting beads (diameter~ 3 mm) were washed with tap water and finally with distilled water to remove excess Ca²⁺ or Fe³⁺ ions on the surface of beads. Cross linking of Fe³⁺ was indicated by the color change of the bead from colorless to yellowish brown.

The FFA composite was prepared using the same method. Instead of agar, alginate (Sisco Research Laboratory chemicals, India) and fly ash from a local dendro power plant was used. For crosslinking, a 5% Cu²⁺ was used by dissolving an appropriate amount of CuSO₄.5H₂O (BDH chemicals England).

Characterization of the composite

Chemical properties of fly ash

The fly ash was obtained from a Dendro-power plant in Sri Lanka and characterized. The content

analysis (BS EN 450:1994) showed: SO₃-1.87%, Cl⁻-0.24%, SiO₂-5.46%, AlO₂-8.11%, Fe₂O₃-1.31%, CaO-31.52%, MgO-7.09%, Na₂O-0.93%, K₂O-5.80% and gravimetric analysis showed 0.03% of moisture content in the fly ash.

Determination of surface area of the composite

Methylene blue solutions were prepared in the concentration range of 1×10^{-6} to 5×10^{-6} mol L⁻¹. A suspension of the adsorbent (50 mg L⁻¹) was stirred for 24 h in 100 mL of methylene blue solution to ensure the formation of a monolayer. The suspension was then centrifuged, and the concentration of the remaining methylene blue solution was determined using UV-Vis spectrophotometer. The average amount of the methylene blue adsorbed onto the surface of the adsorbent at saturation was calculated. The specific surface area (S) was calculated using Equation (1).

$$S = \frac{M_{MB} \times N_A \times A_{MB}}{m} \quad (1)$$

where, M_{MB} is the number of moles of methylene blue adsorbed to complete the monolayer, N_A is the Avogadro's number, A_{MB} is the surface area per methylene blue molecule, and m is the amount of adsorbent in the suspension.

Determination of surface charge of the composite

Nitrogen gas was bubbled through a suspension of 10.00 g L⁻¹ adsorbent in 100.00 mL of 0.1 mol L⁻¹ NaNO₃ solution, with constant stirring, for 3 h. The beaker with the suspension was sealed with parafilm and the stirring continued for another 12 h. The initial pH of the system was then measured, and the pH of the suspension was raised up to pH 10 by addition of 0.1 mol L⁻¹ NaOH in 0.1 mol L⁻¹ NaNO₃. Next, the suspension was titrated against 0.1 mol L⁻¹ HNO₃ in 0.1 mol L⁻¹ NaNO₃ using the potentiometric autotitrator until the pH of the system was below 3. Throughout the titration the system was continuously stirred and purged with N₂ gas. The procedure was repeated with 0.01 mol L⁻¹ and 0.001 mol L⁻¹ NaNO₃.

The surface charge, σ, of the composite was calculated using Equation (2).

$$\sigma = \left(\frac{F}{a \times s} \right) \{ (C_a - C_b) - [H^+] + [OH^-] \} \quad (2)$$

where, F is the Faraday constant (96490 C mol^{-1}), a is the solid content of the suspension in g L^{-1} , s is the specific surface area of the composite in $\text{m}^2 \text{ g}^{-1}$, C_a and C_b are the concentrations of acid and base in the medium at a particular point of titration and H^+ and OH^- are the hydrogen and hydroxide ion concentrations, respectively, in the medium according to the measured pH at a particular point of titration.

FT-IR analysis of the adsorbent

For the preparation of the pellet for FT-IR analysis, analytical grade KBr was fused at 800°C for 3 h in a muffle furnace and cooled gradually to give FT-IR grade KBr. The KBr and composite were mixed in 10:1 ratio and ground in an agate mortar. The KBr pellet for FT-IR was prepared using a small portion of this mixture.

Kinetics study

For the investigation of the kinetics of phosphate adsorption, 0.50 g of the composite was added to 25.0 mL of 5.0 mg L^{-1} phosphate solution in 50 mL centrifuge tubes. The suspension was agitated in a linear shaker and samples of the suspensions were removed at predetermined time intervals. The solution was filtered and the filtrate analyzed for residual phosphate concentration. The data were fitted into pseudo 1st and 2nd order kinetics models.

The adsorption percentage (A%) values were calculated using Equation (3).

$$A\% = \frac{(C_i - C_f)}{C_i} \times 100 \quad (3)$$

where C_i and C_f are the initial and final phosphate concentrations in mg L^{-1} , respectively.

Isotherm study

For the isotherm study, 0.50 g of the composite was agitated with 2.0, 3.0, 5.0, 15.0, 25.0, 40.0, and 50 mg L^{-1} phosphate solutions, while maintaining the initial pH at 5.5. After the samples reached equilibrium, the suspensions were removed, filtered and the residual phosphate

concentration was determined. The data were fitted to Langmuir, Freundlich, Dubinin–Radushkevich, and Langmuir–Freundlich combined isotherm models.

The adsorption capacity q (mg g^{-1}) was calculated using Equation (4):

$$q = (C_i - C_f) \times \frac{V}{M} \quad (4)$$

where V is the volume (mL) of the phosphate solution and M is the mass of the adsorbent (g) and C_i and C_f are the initial and final phosphate concentrations at equilibrium time (mg L^{-1}), respectively.

Adsorption experiments

To determine the adsorption parameters, 0.50 g of the composite was mixed with 25.0 mL of 5.0 mg L^{-1} phosphate solution at pH 5.5 and shaken at 100 rpm in a linear shaker by changing one parameter at a time. To determine the effect of pH on phosphate adsorption, the initial pH of phosphate solution was varied from pH 1.0 to pH 12.0 by adding appropriate quantities of NaOH and HNO_3 . Different dosages of the composite (i.e., 4.0, 8.0, 20.0, 40.0, and 80.0 g L^{-1}) were used to investigate the effect of dosage on phosphate adsorption. To determine the effect of shaking speed on adsorption, the samples were shaken at 50, 100, and 150 rpm. After equilibrium was reached, samples were removed, filtered and the filtrate analyzed for residual phosphate concentration using UV-Visible spectrophotometer. The Gibbs free energy change for adsorption was determined by following the same procedure as for the isotherm study at different temperatures (30, 35, 40, 45°C). Each experiment was independently repeated three times.

Results and discussion

Kinetics study

In the adsorption process, the duration of contact between the phosphate ion and the composite is an important parameter related to both kinetics and equilibrium. The initial process of rapid adsorption was followed by a slower process, due

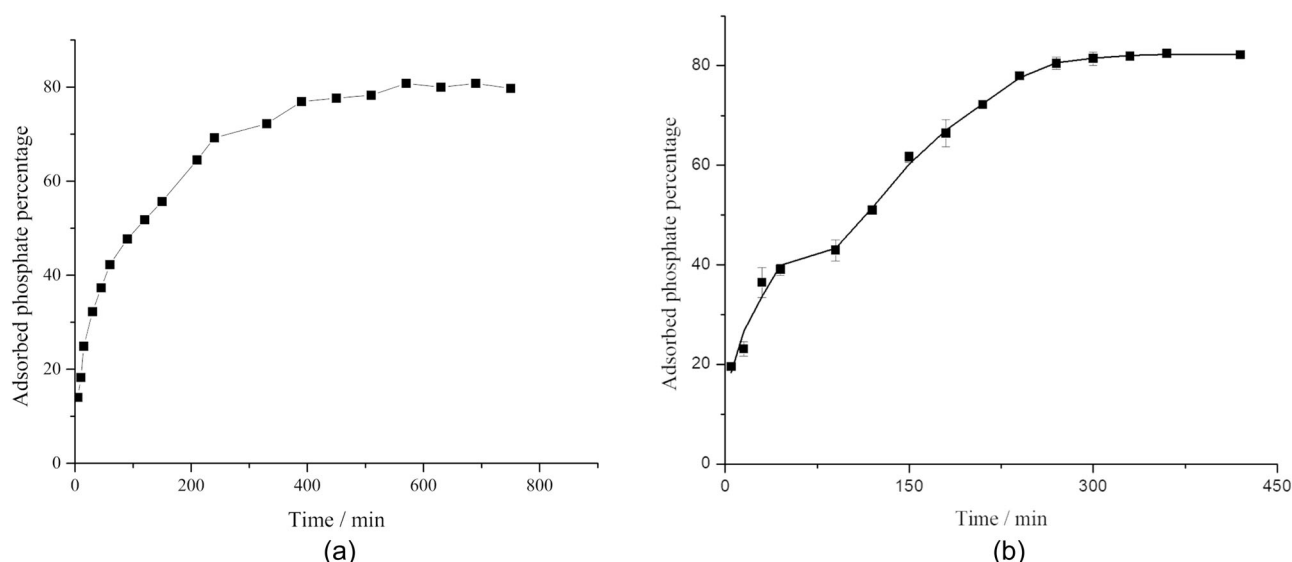


Figure 1. (a) Adsorption of phosphate by the FAA composite with time. Composite (0.5 g) was agitated in 25 mL of 5 mg L⁻¹ phosphate solution at pH 5.5, n = 3. (b) Adsorption of phosphate by the FFA composite with time. Composite (0.5 g) was agitated in 25 mL of 5 mg L⁻¹ phosphate solution at pH 5.5, n = 3.

to continuous occupation of adsorption sites when the interaction of phosphate species with the adsorbent is in progress (Figure 1a). The FAA composite adsorbed 15% of the phosphate ions during the initial rapid phase of 5 min, followed by 69% in the first 4 hours; 81% was adsorbed at equilibrium after 9.5 h. Similarly, the FFA composite adsorbed 20% of phosphate rapidly in the first 5 minutes. However, equilibrium was reached after 5.5 h, much earlier than with FAA composite, yet showing a similar maximum adsorption (83%) (Figure 1b). Similar results were reported for phosphate adsorption by dual Zr and La hydroxide/cellulose based biocomposites (Du et al. 2019), chemically modified carbonaceous clay (Selim, Sellaoui, and Mobarak 2019) and alginate/iron(III) chloride capsule (Siwek et al. 2016). In the initial rapid phase of adsorption, phosphate ions bind to the active surface sites, which are available in abundance (Wang et al. 2013; Jiang et al. 2013). When the phosphate ion is adsorbed, the surface of the composite becomes negatively charged, thus resulting in a decrease in the adsorption rate (Luengo et al. 2006) due to the electrostatic repulsion of the negatively charged surface and the negative phosphate ions. For better understanding of the kinetics, data from contact time experiments were fitted to pseudo 1st and 2nd kinetic models.

Kinetics models

The experimental data obtained for phosphate adsorption were fitted into two fundamental kinetics models and two rate controlling models to understand the adsorption process. The pseudo 1st and 2nd order non-linear kinetic models can be expressed as Equations (5) and (6), respectively (Blanchard, Maunaye, and Martin 1984; Lagergren 1898)

$$q_t = q_e(1 - e^{-k_1 t}) \quad (5)$$

$$q_t = \frac{k_2 q_e^2 t}{1 + k_2 q_e t} \quad (6)$$

where q_t is the amount of solute adsorbed (mg g⁻¹) on the adsorbent at time t and q_e is the amount of the solute adsorbed (mg g⁻¹) on the adsorbent at equilibrium, while k_1 (min⁻¹) and k_2 (g mg⁻¹ min⁻¹) are the pseudo 1st and 2nd order constants, respectively.

The pseudo 2nd order model is chosen to describe the process of adsorption of PO₄³⁻ onto FAA composite, since it has a high regression coefficient (R^2) of 0.964 (Supplementary material Figure S1, Table 1) and the q_e calculated (0.175 mg g⁻¹) is closer to the q_e value obtained experimentally (Table 1). The FFA composite also showed better agreement with the pseudo 2nd order kinetic model with R^2 value of 0.941 and a q_e value of 0.136 mg g⁻¹ which is closer to the experimental value (Supplementary

Table 1. Parameters calculated for different kinetic models for adsorption of PO_4^{3-} onto FAA and FFA composites (initial concentration 5.0 mg L^{-1} , initial pH 5.5, shaking speed = 100 rpm, temperature 27°C , $n = 3$).

Adsorbent	Biomass	$q_{e(\text{exp})}$	Pseudo 1 st order			Pseudo 2 nd order		
			k_1	q_e	R^2	k_2	q_e	R^2
FAA	0.50	0.17	0.013	0.153	0.911	0.098	0.175	0.964
FFA	0.50	0.11	0.014	0.112	0.906	0.122	0.136	0.941

See text for abbreviations.

material Figure S2, Table 1). This agreement with the pseudo 2nd order model indicates a chemisorption process. Therefore, it can be assumed that the phosphate removal from the aqueous solution is due to a chemical interaction with the adsorbent surface. The composite surface is rich in functional groups and Ca^{2+} and Fe^{3+} ions from the crosslinking of the feldspar-alginate-agar. In FAA composite, the two biopolymers, agar and alginate, have functional groups such as sulfite, carboxylic acid, hydroxyls and methylene groups (Soares et al. 2004; Singh et al. 2014; Lahaye and Rochas 1991b). Therefore, the adsorption benefits from ion exchange and covalent interaction due to sharing or exchange of electrons between phosphate ion and the composite surface (Ho 2006). Phosphate adsorption that follows the pseudo 2nd order model has been reported for adsorption onto several other synthetic materials (Pan et al. 2017; Ogata et al. 2017; Lin et al. 2017; Wang et al. 2017; Xiong et al. 2017; Wang et al. 2016). Therefore, the long period of time required for the adsorption process could be due to the necessity for collision of phosphate ions with the composite surface and chemical interaction between phosphate ions and Ca^{2+} and Fe^{3+} ions (Mao and Yue 2016).

Diffusion models

Kinetics of the adsorption process is governed by how fast the adsorbate diffuses through the liquid film and immobilize the functional groups of the surface after intraparticle diffusion. Therefore, kinetics data were fitted to intra-particle diffusion and liquid film diffusion models to determine the rate controlling steps. These two models can be expressed as Equations (7) and (8), respectively (Weber and Morris 1963; Qiu et al. 2009).

$$q_t = k_i t^{0.5} \quad (7)$$

$$\ln\left(1 - \frac{q_t}{q_e}\right) = -R^l t \quad (8)$$

where k_i and R^l are intra-particle diffusion constant ($\text{mg g}^{-1} \text{min}^{-0.5}$) and liquid film diffusion constant (min^{-1}), respectively. Liquid film diffusion constant R^l can be further expressed as,

$$R^l = \frac{3D_e^l}{r_0 \Delta r_0 k^l} \quad (9)$$

where D_e^l is the effective liquid film diffusion coefficient ($\text{cm}^2 \text{min}^{-1}$), r_0 is the radius of the adsorbent (cm), Δr_0 is the thickness of the liquid film (cm), and k^l is the adsorption equilibrium constant.

When the data from PO_4^{3-} adsorption onto FAA composite were fitted to the intra-particle diffusion model, the resulting graph (Figure 2a) gave an R^2 of 0.9410 with an intra-particle diffusion constant of $0.006 \text{ mg g}^{-1} \text{min}^{-0.5}$ (Table 2). Similar behavior was observed for the PO_4^{3-} adsorption onto FFA composite, with a R^2 of 0.995 and a rate constant of $0.0063 \text{ mg g}^{-1} \text{min}^{-0.5}$ (Figure 2b).

The latter part of the graph (Figure 2a,b) showed a decrease in the slope due to the low availability of phosphate ions in the bulk solution and the concentration gradient between the solid phase and liquid phase. The rate limiting step of this adsorption process is not only the intra-particle diffusion model since the straight line did not pass through the origin. There may be other rate limiting steps involved in the adsorption process to control the rate of phosphate adsorption. Therefore, the data were fitted to a liquid film diffusion model (Figure 2c,d) to determine whether the rate controlling step is due to the movement of phosphate ions from the liquid phase to the solid phase. The plot for FAA composite gave a straight line with a high R^2 (0.9898) and a negative gradient (Table 2). Thus, it is suggested from this study, that the rate limiting step of the adsorption process depends on both intra-particle diffusion and film diffusion. However, liquid film diffusion occurs in two steps when PO_4^{3-} is adsorbed onto FFA. Initially, the rate of diffusion through the liquid film is slow (-0.0067 min^{-1}) which is followed by a faster

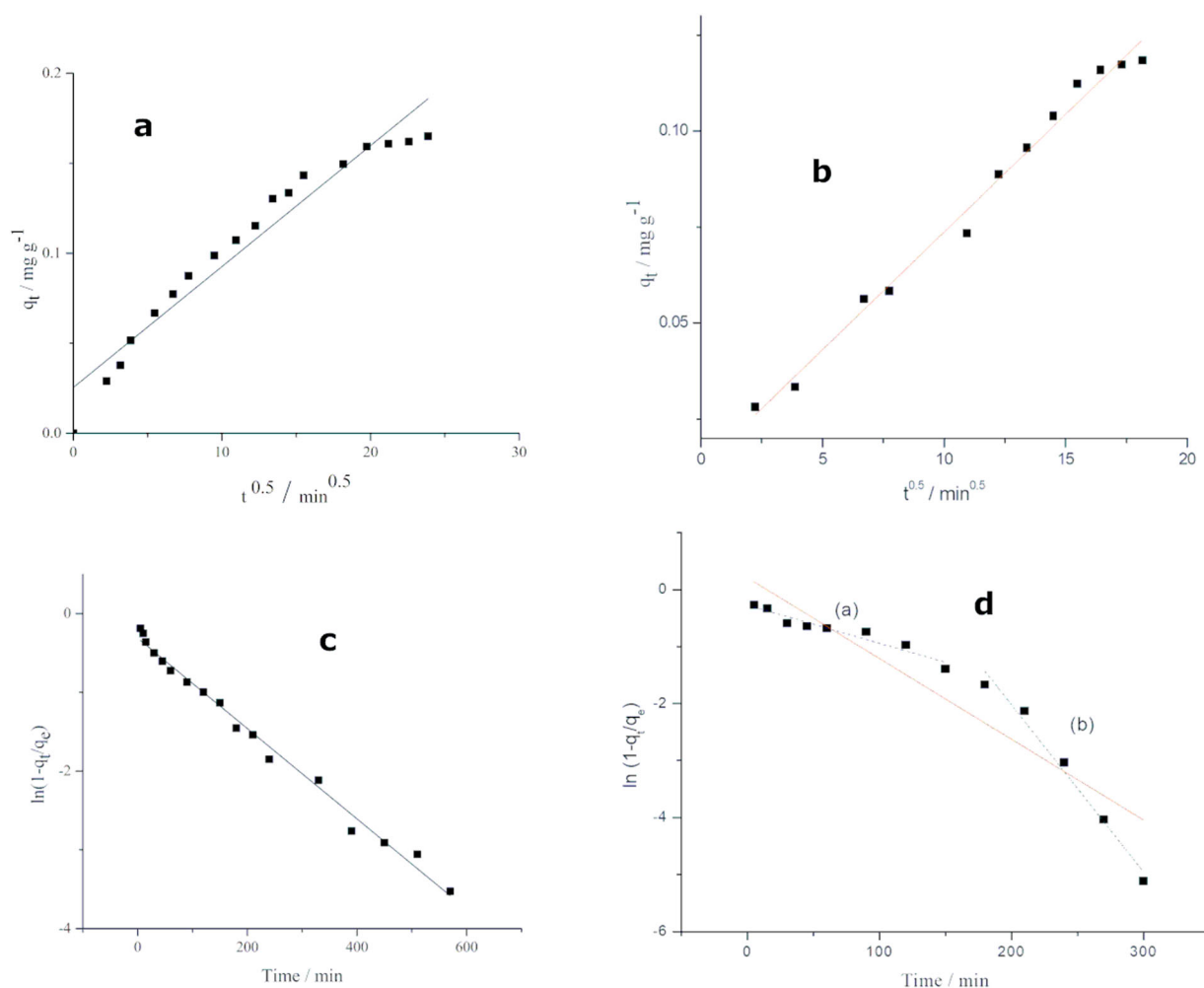


Figure 2. Plot of intra-particle diffusion model for the adsorption of PO_4^{3-} by the (a) FAA (b) FFA composites and plot of liquid film diffusion model of PO_4^{3-} by the (c) FAA (d) FFA composites (Initial pH 5.5, temperature 25°C , composite dose 20.0 g L^{-1} , initial phosphate concentration 5 mg L^{-1} , $n = 3$).

Table 2. Parameters calculated for different diffusion models for adsorption of PO_4^{3-} onto FAA and FFA composites (initial concentration 5.0 mg L^{-1} , initial pH 5.5, shaking speed = 100 rpm , temperature 27°C , $n = 3$).

Adsorbent	Biomass	Intraparticle			Liquid film	
		k_{int}	Intercept	R^2	R^1	R^2
FAA	0.50	0.006	0.025	0.941	-0.005	0.989
FFA	0.50	0.0063	0.012	0.995	-0.014	0.870
FFA phase 1					-0.006	0.916
FFA phase 2					-0.029	0.976

NA – Not Applicable.
See text for abbreviations.

second step with a rate of -0.029 min^{-1} (Figure 3d). Adsorption occurs by diffusion of phosphate ions through the liquid film around the adsorbate particles and thereafter by diffusion of the phosphate ions to the active sites within the adsorbent surface.

pH and phosphate adsorption

The pH of the solution determines the surface properties of the composite and bulk properties of the solution (Wang et al. 2017). When the pH of the solution is low, the surface becomes positively charged. The maximum phosphate adsorption of more than 80% onto FAA composite was observed in the pH range 4–10. There were three distinct phases of phosphate adsorption by the composite (Figure 3a). Similarly, phosphate adsorption onto FFA composite showed a maximum adsorption (76–85%) between pH 3–7. The adsorption of phosphate in highly acidic pH, (< 2), was low, steadily increasing with increasing pH up to 4 and remaining more or less constant thereafter. The adsorption curve sharply declined from pH 10 and continued up to pH 12 for FAA

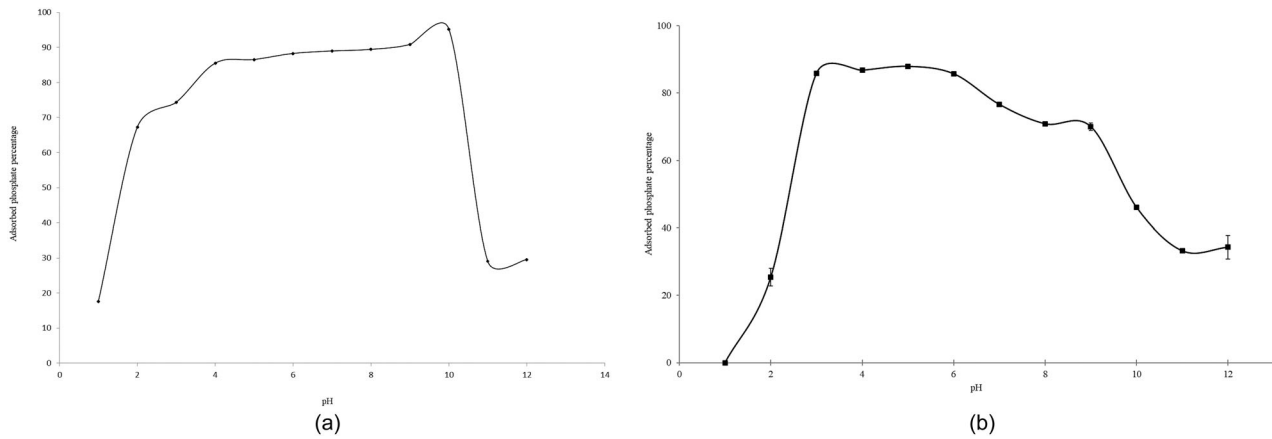
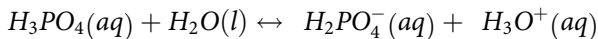


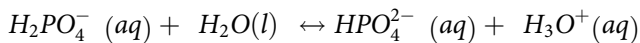
Figure 3. (a) Adsorption of phosphate by the FAA composite composites at different initial pH values. Adsorption conditions were temperature 25 °C, composite dose 20.0 g L⁻¹, initial phosphate concentration 5 mg L⁻¹, number of replicates 3. (b) Adsorption of phosphate by the FFA composite composites at different initial pH values. Adsorption conditions were temperature 25 °C, composite dose 20.0 g L⁻¹, initial phosphate concentration 5 mg L⁻¹, number of replicates 3.

composite while for FFA composite, the decline takes place after pH 7 (Figure 3b).

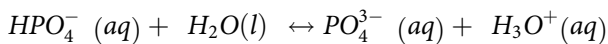
With pK values of 2.15 (pK₁), 7.20 (pK₂), and 12.33 (pK₃), the phosphate ion can exist as H₂PO₄⁻, HPO₄²⁻, and PO₄³⁻ (Eqs. 8–10). In a solution with pH < 2, between pH 2–6, pH 8–12, and pH > 12, the predominant species are H₃PO₄, H₂PO₄⁻, HPO₄²⁻, and PO₄³⁻, respectively. Thus, the solution pH determines the principal phosphate species present in the solution affecting the electrostatic interaction between phosphate species and the composite surface, and hence, the speciation of the phosphate ion.



$$\text{pK}_1 = 2.15 \quad (10)$$



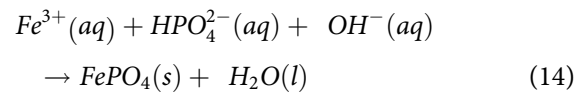
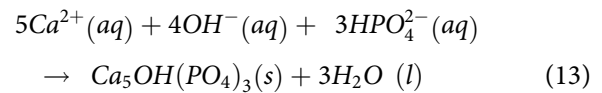
$$\text{pK}_2 = 7.20 \quad (11)$$



$$\text{pK}_3 = 12.33 \quad (12)$$

Since HPO₄²⁻ is predominant in the pH range 4–10, the HPO₄²⁻ ion is attracted toward the composite. The presence of Ca²⁺ ions thus leads to the precipitation of hydroxylapatite, as shown in Equation (13). Phosphate removal was more efficient in pH range 4–10 with their adsorption onto polymers, followed by the formation of

precipitates with Ca²⁺ and Fe³⁺ ions (Equations (13) and (14)).



Below pH 4, the H₃PO₄ species is dominant, which would neither show electrostatic attraction nor ion exchange with the composite, thus lowering phosphate adsorption. In the pH range 4–8, the composite surface becomes positively charged, attracting negatively charged phosphate ions, thus showing greater adsorption. At higher pH (> 10), the adsorbent surface is negatively charged, initiating the electrostatic repulsion with phosphate anion, which decreases the extent of adsorption.

Composite dosage and shaking speed

Both the adsorbent dosage and shaking speed have a direct influence on adsorption. The former determines the availability of active sites for adsorption while the latter provides sufficient energy for adsorption through collisions. With increasing dosage of the FAA composite from 0.1 g to 2.0 g, adsorption increased from 15% to 96%, whereas similar increase of dosage of FFA composite increased the absorption percentage from 50% to 90%. This observation can be

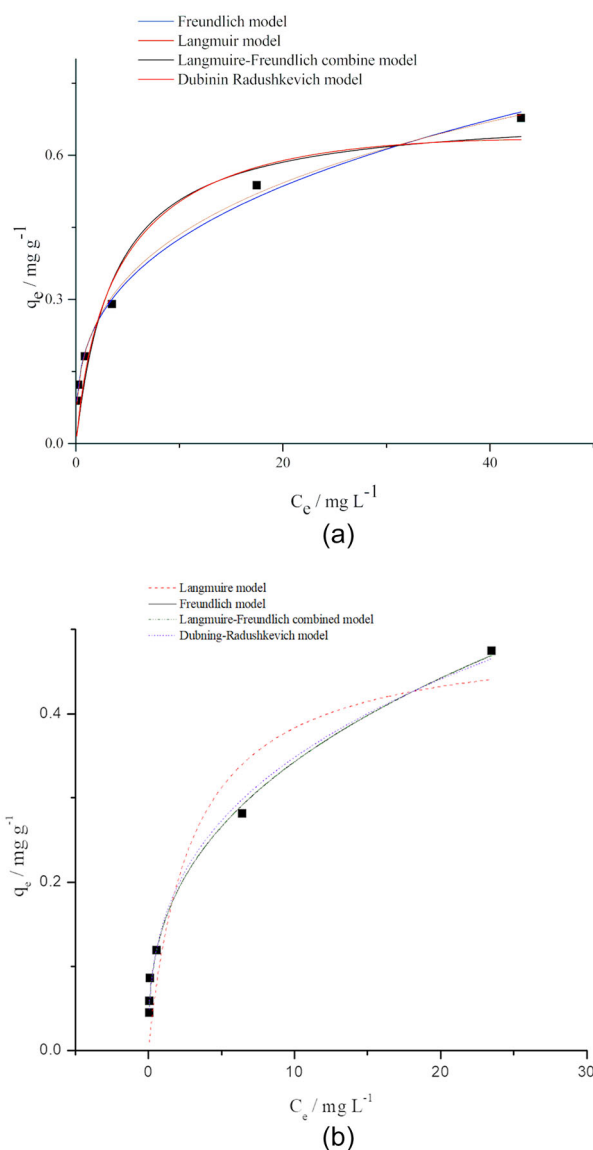


Figure 4. (a) Isotherm curves for PO_4^{3-} adsorption onto 0.50 g of FAA composite at pH 5.0 at 27°C temperature (shaking speed 100 rpm, $n=3$). (b) Isotherm curves for PO_4^{3-} adsorption onto 0.50 g of FFA composite at pH 5.0 at 27°C temperature (shaking speed 100 rpm, $n=3$).

attributed to the fact that when the adsorbent dose increases, active sites available for the adsorption of phosphate also increases. With the availability of excess surface for binding, competition between phosphate ions and other ions for the active sites is reduced. The rate limiting steps for the adsorption of phosphates are the transfer of the phosphate in the solution into the composite's outermost liquid layer, and moving to the immediate surface active sites of the composite (Baral et al. 2009). Adsorption of phosphate onto the composite is governed by these two factors. Therefore, when the shaking speed increases,

collisions of phosphate ions with the composite surface also increase, thereby increasing the adsorption from 74% (at 50 rpm) to 81% (at 100 rpm) for FAA composite. When the shaking speed is too high (rpm 150), the time available is limited for interaction between the adsorbent and phosphate ions. Therefore, adsorption does not take place effectively. This explains the lower adsorption (77%) at 150 rpm, compared to that at 100 rpm. However, for the FFA composite, PO_4^{3-} adsorption was only 20% without shaking the system, and the maximum adsorption of 80% was observed at 50 to 150 rpm shaking speeds.

Isotherm study

An isotherm study was conducted to determine the interactions between phosphate ions and the composite. At equilibrium, the amount of solute adsorbed onto the adsorbent is the same as the amount of solute desorbed into the solution. The amount of phosphate adsorbed, q_e (mg g^{-1}), on the adsorbent as a function of equilibrium or remaining concentration of phosphate, C_e (mg L^{-1}) in solution is shown in Figure 4. The data were fitted to Langmuir, Freundlich, Dubinin–Radushkevich, and Langmuir–Freundlich combined isotherm models, which are briefly described below.

The Langmuir model (Equation (15)) predicts monolayer adsorption at predetermined definite active sites on the homogenous surface of the adsorbent (Langmuir 1918).

$$q_e = \frac{q_0 K_L C_e}{1 + K_L C_e} \quad (15)$$

where, q_0 is the maximum adsorption capacity (mg g^{-1}), which is equivalent to complete monolayer surface coverage and K_L is the Langmuir constant (L mg^{-1}).

The adsorption intensity can be calculated using Equation (16).

$$R_L = \frac{1}{1 + K_L C_i} \quad (16)$$

where, for favorable adsorption, $0 < R_L < 1$, unfavorable adsorption $R_L > 1$, linear adsorption $R_L=1$ and irreversible adsorption $R_L = 0$.

The Freundlich model (Equation (17)) describes a reversible, multilayer adsorption on a

Table 3. Adsorption isotherm parameters for PO_4^{3-} adsorption onto 0.50 g of FAA and FFA composite adsorbents (temperature = 27 °C, pH= 5.5, shaking speed= 100 rpm, $n = 3$).

Adsorbent	Model	k	q_0	n	E	C_s	R^2
FAA	Langmuir	0.27	0.69	NA	NA	NA	0.914
	Freundlich	0.19	NA	3.02	NA	NA	0.995
	Dubinin–Radushkevich	7.35×10^{-9}	0.63	NA	48.8	−8.25	0.999
	Langmuir–Freundlich	0.27	0.69	1	NA	NA	1
FFA	Langmuir	0.34	0.49	NA	NA	NA	0.877
	Freundlich	0.15	NA	2.72	NA	NA	0.993
	Dubinin–Radushkevich	6.09×10^{-10}	NA	NA	8.07×10^{10}	28.64	0.987
	Langmuir–Freundlich	1.25×10^{-7}	51.91	0.36	NA	NA	0.991

NA – Not applicable.

See text for abbreviations.

heterogeneous surface (Freundlich 1906). This exponential equation predicts that the adsorption of the solute onto the adsorbent surface increases with the solute concentration.

$$q_e = K_F C_e^{1/n} \quad (17)$$

where K_F is the Freundlich constant and n is the surface heterogeneity.

The Langmuir–Freundlich combined model (Equation (18)) relates to the concentration of adsorbed and free phosphate ions in solution. This model envisages that at high sorbate concentration, the adsorption is reduced to a monolayer following the Langmuir isotherm and at low sorbate concentration, adsorption obeys the Freundlich model.

$$q_e = \frac{q_0 (K_{LF} C_e)^n}{(K_{LF} C_e)^n + 1} \quad (18)$$

where K_{LF} is the Langmuir–Freundlich isotherm constant (L mg^{-1}) for heterogeneous solid and n is the Langmuir–Freundlich heterogeneity parameter. The value of n varies between 0 and 1, where $n = 1$ for homogeneous materials and $n < 1$ for heterogeneous materials (Jeppu and Clement 2012).

The Dubinin–Radushkevich model (Equation (19)) is based on the adsorption energies and heterogeneity of the surface of adsorbent (Dubinin and Radushkevich 1947). It assumes that the sorption depends on the porous structure of the adsorbent material (Zhao and Feng 2016).

$$q_e = q_0 \exp \left\{ - \left[\frac{RT \ln \left(C_s / C_e \right)}{E} \right]^2 \right\} \quad (19)$$

$$E = \frac{1}{\sqrt{2\beta}}$$

where C_s is the saturation concentration of

phosphate (mg L^{-1}), R is the universal gas constant ($8.314 \text{ J K}^{-1} \text{ mol}^{-1}$), T is the absolute temperature (K), E is the mean free energy per molecule of adsorbent (kJ mol^{-1}) and β is the Dubinin–Radushkevich constant ($\text{mol}^2 \text{ J}^{-2}$) and is described as the free energy of transfer of 1 mol of solute in the solution from an infinite distance to the surface of the adsorbent. This model can be used to determine the adsorption mechanism using the value of E . If E lies between 1 and 8, the process of interaction is considered to be physical adsorption or ion exchange, while chemical sorption occurs if it is between 9 and 16 (Pan et al. 2017).

The data for PO_4^{3-} adsorption, onto FAA and FFA composites, fitted well to all four isotherm models with high R^2 values from 0.91 to 1.0, and 0.87 to 0.99, respectively (Table 3). The Freundlich isotherm model showed relatively high R^2 of 0.995 and 0.993 for FAA and FFA composites, respectively. The Freundlich model predicts adsorption onto heterogeneous surfaces with different adsorption energies to form a multilayer (Liu et al. 2016); hence the adsorption process is physical. The FAA composite surface in this study is rich in hydroxyl groups, with Ca^{2+} and Fe^{3+} ions whereas FFA surface is rich in Cu^{2+} and ions present in fly ash making the surface heterogeneous. According to this model, adsorption is favorable when $0 < 1/n < 1$ (where n = surface heterogeneity). Since $1/n$ in this study is 0.33 and 0.36 for FAA and FFA composites, respectively, it can be concluded that the adsorption is favorable for a multilayer adsorption of phosphate ions. The R^2 value for the Langmuir–Freundlich isotherm was reported as 1.00 for FAA composite and 0.991 for FFA composite. Since the heterogeneity parameter, n , of

the Langmuir–Freundlich combined model calculated for the FAA composite is 1.0, the equation is reduced to the Langmuir model, which predicts that the adsorption gives rise to a monolayer onto a homogeneous surface. This happens after the phosphate ions react with Ca^{2+} and Fe^{3+} and form precipitates, leaving only hydroxyl groups on the surface. This makes the surface to be homogeneous with the same activation energies. Thereafter, it can be assumed that the adsorption of phosphate takes place onto a homogeneous surface following the Langmuir model. The heterogeneity parameter for the FFA composite is calculated as 0.36, and the maximum adsorption capacity q_0 was 51.91 mg g^{-1} . The Langmuir–Freundlich constant was $1.25 \times 10^{-7} \text{ L mg}^{-1}$. As this model states, when the phosphate concentration is high, the adsorption follows Langmuir model with a monolayer formation and when the phosphate concentration is low the adsorption is reduced to Freundlich model. These observations can be justified by the maximum adsorption capacity values obtained for both models. The Dubinin–Radushkevich model is based on the temperature dependence of adsorption on its energies (Zhao and Feng 2016). The phosphate adsorption onto the FAA composite agreed with the Dubinin–Radushkevich model with R^2 of 0.999 whereas, it was 0.991 for FFA composite. Adsorption can be assumed to have taken place onto a heterogeneous porous material, as assumed by this model. The mean free energy per molecule of adsorbent was $-8.25 \text{ kJ mol}^{-1}$, a value slightly higher than the mean free energy for a physical sorption process. For the FFA composite, the mean free energy is $28.64 \text{ kJ mol}^{-1}$, which is a chemical process. According to the postulations made for the Langmuir–Freundlich combined model, the formation of $\text{Ca}_5\text{OH}(\text{PO}_4)_3$ and FePO_4 is a chemical process, which requires a drop in the mean free energy. Since the second step of the adsorption process involved weak physical interactions, such as H-bonding and ion exchange, the mean free energy is lowered. Therefore the adsorption process is physical sorption with ion exchange mechanisms (Pan et al. 2017). However, fly ash contains Al, Ca, Fe, Mg, and Ti as components which can form precipitates besides Cu which

can form $\text{Cu}_3(\text{PO}_4)_2$ and the process is more chemical in nature. The overall conclusion is that the phosphate ion is initially adsorbed onto a heterogeneous surface followed by the formation of precipitates with metal cations. After the composite surface becomes homogenous, due to metal phosphate precipitation, which covers the adsorbent surface, adsorption occurs through physical interactions between the functional groups of the adsorbent and the remaining PO_4^{3-} ions.

Thermodynamic study

The thermodynamic parameters were calculated for the adsorption of PO_4^{3-} onto FFA composite. Adsorption involves changes in thermodynamic function. To study the temperature dependence of the adsorption process, a thermodynamic study was carried out. A change in temperature can affect the adsorption process in that increasing temperature increases the rate of diffusion of phosphate ions across the external boundary layer and in the internal pores of the composite (Wang et al. 2005). It also changes the equilibrium capacity of the adsorbent (Wang et al. 2005). To investigate the energy effect on adsorption, several thermodynamic parameters have been introduced, including ΔG , ΔH , and ΔS . The thermodynamic parameters were calculated according to the thermodynamic laws. The values for the ΔH and ΔS were obtained from the intercept and slope, respectively, from the graph of ΔG vs temperature.

The temperature of the system showed a direct influence on adsorption. When the temperature increased from 25°C to 30°C , the adsorption of phosphate also increased for all concentrations. Adsorption decreased with increasing phosphate concentration at 25°C . At 25°C the maximum adsorption for phosphate concentrations of 1 mg L^{-1} , 3 mg L^{-1} , 5 mg L^{-1} , and 15 mg L^{-1} were 95%, 80%, 62%, and 47%, respectively. At 30°C , the adsorption for the same set of concentrations was 91%, 89%, 87%, and 85%, respectively. Thereafter, temperature increment did not affect the adsorption. The trend of increasing adsorption percentage with increasing temperature indicates a chemisorption process in the adsorption

Table 4. Values of the thermodynamic parameters of the PO_4^{3-} adsorption by FFA (Initial concentration = 5.0 mg L^{-1} , shaking speed 100 rpm, contact time 330 min).

T (K)	b	ΔG	ΔH	ΔS
298	2065.79	−18.91	16.36	−0.12
303	2450.99	−19.66		
308	2756.88	−20.28		
318	3173.52	−21.32		

See text for abbreviations.

mechanism (Li et al. 2006). The higher adsorption percentage with increasing temperature can be explained by the increased mobility of ions in the solution and also the greater probability of collision between phosphate ions and the composite surface active sites (Goscianska et al. 2018).

When the temperature increases from 298 K to 318 K, the Gibbs free energy change decreases from $-18.91 \text{ kJ mol}^{-1}$ to $-21.32 \text{ kJ mol}^{-1}$ (Table 4). The negative ΔG and positive ΔH values indicate the attainable and endothermic nature of the adsorption (Pan et al. 2017). The negative values of ΔG at all the different temperatures indicate the spontaneous nature of the adsorption (Das et al. 2006; Tran, You, and Chao 2016). The increase of the absolute value of the free energy implies that the higher temperatures are favorable for the adsorption process (Yazdani et al. 2012). This explains the increase in adsorption percentage with the increase of temperature. The positive value obtained for the ΔH reflects the endothermic nature of the adsorption process (Tran, You, and Chao 2016). The ΔH was less than 40 kJ mol^{-1} and therefore the adsorption of phosphate onto FFA is physisorption (Rodrigues and da Silva 2010). As adsorption takes place, the system gains energy in the form of heat from its surrounding. The endothermic circumstances of the adsorption are that the formation of the bonds among the phosphate ions and the active groups on the composite surface requires more energy than the energy released in the bond breaking between phosphate ion-water and cross-linked metal ion-alginate. Therefore, the requirement of excess heat is gained from the surrounding. The endothermic process is enhanced by the increased temperature and therefore the adsorption percentage is high at higher temperature.

The sign of the ΔS can be used to predict the associative/dissociative nature of the adsorption mechanism (Tran, You, and Chao 2016). A

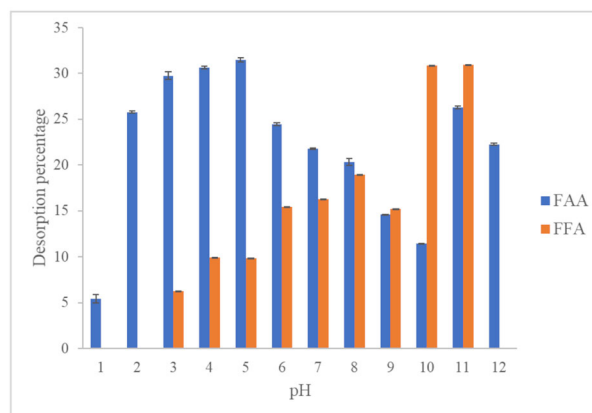


Figure 5. Percentage desorption of phosphate from FFA and FAA composites with different pH solutions.

negative ΔS implies that the adsorption mechanism is associative. The magnitude of ΔS is $-0.12 \text{ kJ mol}^{-1} \text{ K}^{-1}$ and this suggests that the adsorbate solid-solution interface becomes less disordered during the adsorption.

Recovery of the adsorbed phosphates

Recovery of adsorbed phosphate is a critical feature in the reuse of the phosphate as well as the adsorbent. Recycling of the adsorbent would reduce cost. A desorption study for both composites was carried out at different pH. First, the composite was allowed to reach equilibrium for maximum phosphate adsorption. Then it was washed with deionized water to remove the surface phosphate solution. Next, the pH series from pH 1 to 12 was prepared using HCl and NaOH solutions. Then the composite was added and agitated for 24 h in a linear shaker.

Composite FAA showed desorption from pH 1 to 12, without destroying the composite. The highest desorption percentage ($>29\%$) was recorded from pH 3 to 5. In FFA, the composite was destroyed at extreme pH values of 1, 2, and 12. The highest desorption percentage observed was $>30\%$ at pH 10 and 11. Future research will focus on developing efficient desorption with other reagents and reusability of the composite (Figure 5).

Characterization of composite

The Scanning Electron Microscopic (SEM) images of the feldspar and composite before and after

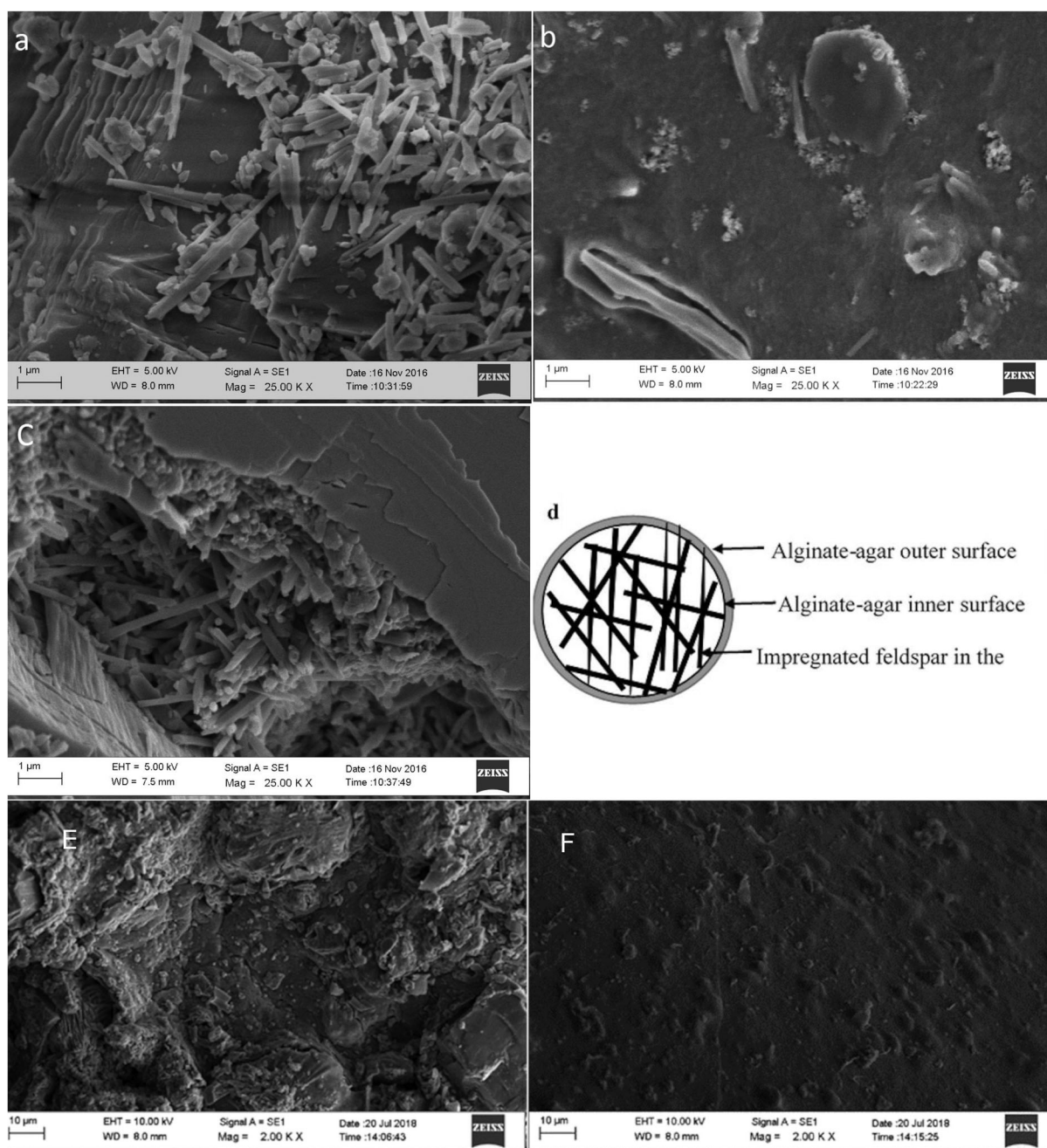


Figure 6. Scanning Electron Microscopic images of (a) Feldspar, (b) Feldspar-agar-alginate composite, (c) Phosphate treated composite (I) feldspar and (II) bound or precipitated phosphate masses and (d) schematic diagram of the composite (e) FFA composite before (f) FFA composite, after phosphate adsorption.

phosphate adsorption are shown in Figure 6. The elongated feldspar particles are of dimensions 1–2 μm (Figure 6a). The feldspar surface coated with agar and alginate was smooth (Figure 6b). The cross section shown in Figure 6c illustrates that the feldspar particles (Figure 6c-I) are impregnated within the biopolymer spheres. Feldspar was included in the composite to achieve a rigid spherical shape with the biopolymer

(Figure 6c). Spherical masses can be seen on the inner surface of the composite (Figure 6c-II) after phosphate adsorption, possibly due to phosphate precipitated with Fe^{3+} or Ca^{2+} . Therefore, it is presumed that phosphate ions diffuse through the polymer layer into the sphere, forming precipitates with free Fe^{3+} and Ca^{2+} ions.

The surface of the FFA before phosphate treatment is relatively smooth, layer-like and flat in

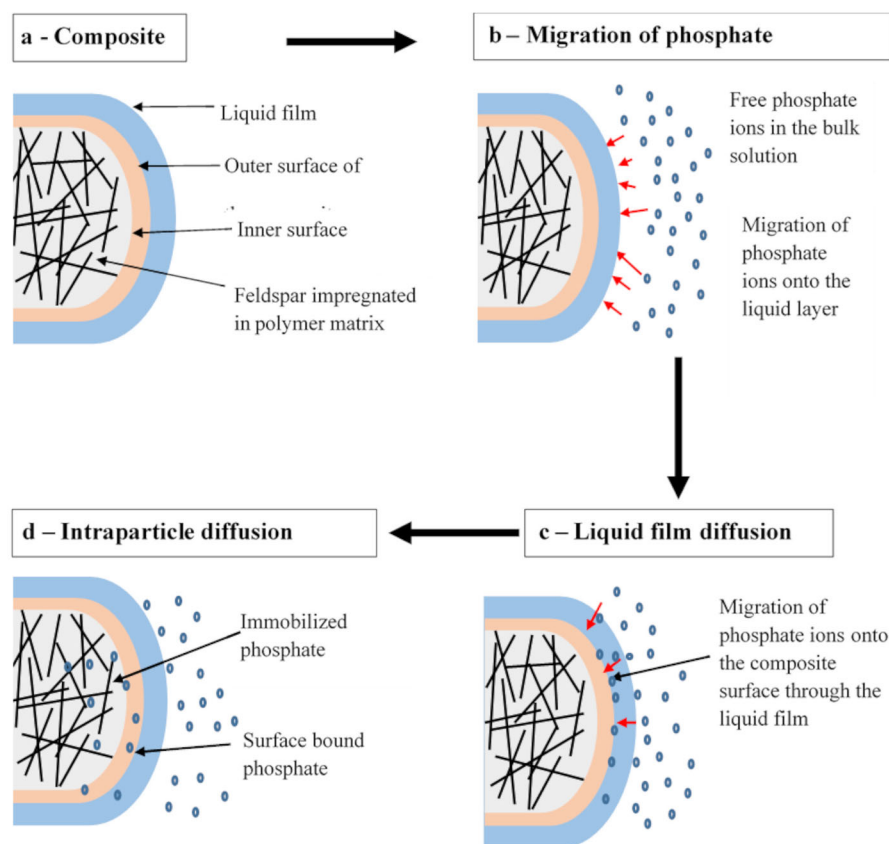


Figure 7. Schematic diagram for the proposed mechanism of phosphate adsorption by the composites.

contrast to that after phosphate treatment, as shown in Figure 6e and f, respectively. After the composite was treated with phosphate, the layer-like structure disappeared and the surface was covered with spherical clusters (Figure 6f). This gives clear evidence of phosphates attached or precipitated with Cu^{2+} . The layer-like surface provides lower surface area for the adsorption of phosphate. This is in good agreement with the surface area of FFA calculated ($2.58 \text{ m}^2 \text{ g}^{-1}$) using methylene blue adsorption method.

The specific surface area of the composite was determined by the methylene blue adsorption method. The average amount of methylene blue adsorbed onto the composite was $1.58 \times 10^{-7} \text{ mol}$. Using this number of moles, the specific surface area of the FFA composite was calculated to be $1.24 \text{ m}^2 \text{ g}^{-1}$. The curves of surface charge density of FFA composite with pH at the three ionic strengths of NaNO_3 intersected at a common point of pH 4, which is the point of zero charge (Dissanayake et al. 2016). At this pH, the surface of the composite is neutral. Below pH 4, the composite surface is positively charged and beyond

this pH, the surface is negatively charged (Supplementary material Figure S3). The surface charge of the adsorbent surface affects the adsorption percentage up to some extent, but does not completely eliminate the adsorption of phosphate in the entire pH range (Luo et al. 2016).

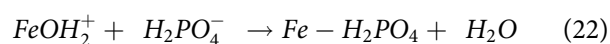
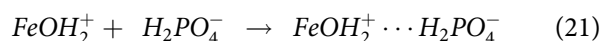
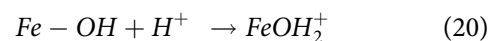
The average amount of methylene blue adsorbed onto the FFA composite was $3.3 \times 10^{-8} \text{ mol}$. The calculated specific surface area of the FFA composite was $0.26 \text{ m}^2 \text{ g}^{-1}$. This may suggest the low porosity of the composite with some large pores. The three curves of surface charge density of FFA composite with pH at different NaNO_3 ionic strengths intersected at pH 6.6, which is the point of zero charge (Supplementary material Figure S4). Below this pH the composite surface is positively charged and above this pH the surface is negatively charged. The optimum pH for phosphate adsorption by FFA was recorded in the pH range 3–7. This observation is supported by the point of zero charge at pH 6.6. When the pH increased beyond 7, the surface is charged negatively, and it repels the phosphate ions.

The FT-IR spectrum of FAA indicates that the functional groups present in the composite are H-bonded hydroxyl groups (3435 cm^{-1}), carbonyl groups (1709 cm^{-1}), carboxylate groups (1539 cm^{-1}) (Liu et al. 2016), C-H bending of alkane groups (1404 cm^{-1}) and ether groups (1035 cm^{-1}) (Silverstein and Bassler 1962; Pavia et al. 2008) (Supplementary material Figure S5). After adsorption of phosphate, the peaks corresponding to the H bonded hydroxyl groups, carbonyl groups and alkane groups were shifted to 3429 cm^{-1} , 1730 cm^{-1} , and 1414 cm^{-1} , respectively (Supplementary material Figure S6), indicating that these functional groups are involved in phosphate adsorption. Supplementary material Figure S6 shows the FTIR spectrum of the FFA composite before and after phosphate adsorption. The broad band at the $3600\text{--}3100\text{ cm}^{-1}$ region is assigned to the stretching vibrations of hydroxyl group (Gu et al. 2017). The peak at 1384 cm^{-1} is attributed to the OH group on the surface of the FFA composite with the Cu^{2+} (Gu et al. 2017) and after the phosphate adsorption this peak is weakened. This suggests that the phosphate ion is directly coordinated to the metal ion. New peaks appear at 1060 cm^{-1} and 562 cm^{-1} which are due to the presence PO_4^{3-} (Ye et al. 2015).

Proposed mechanism of phosphate adsorption by feldspar-alginate-agar composite

From the kinetic and isotherm data for the adsorption process, we propose the following mechanism for phosphate adsorption by the feldspar-alginate-agar composite. First, phosphate ions migrate from the bulk solution to the boundary liquid layer of the composite as suggested by the liquid film diffusion model (Figure 7b). Then the phosphate ions are precipitated as FePO_4 , $\text{Ca}_3(\text{PO}_4)_2$, and $\text{Ca}_5\text{OH}(\text{PO}_4)_3$ with the available Ca^{2+} and Fe^{3+} ions on the composite surface. This precipitation makes the surface to be homogenous. The phosphate ions then migrate to the surface active sites of alginate and agar polymers as suggested by the intraparticle diffusion model (Figure 7c) and these complexes can entrap phosphate ions through H and covalent bonding. The remaining phosphate ions migrate to the interior active sites of the

composites where the biopolymers contribute to entrapping phosphate ions. Ferric and calcium ions present in the alginate- $\text{Fe}^{3+}/\text{Ca}^{2+}$ matrix could precipitate phosphate as given by Equations (8) and (9). (Figure 7d). Ferric ions in the composite can exist in its protonated form and could play a major role in H_2PO_4^- adsorption by electrostatic attraction and ligand exchange mechanisms (Equations (20)–(22)) (Zhang et al. 2017). Therefore, phosphate adsorption occurs through physical and chemical interactions making the adsorption a complex process.



Proposed mechanism of phosphate adsorption by feldspar-flyash-agar composite

Uptake of phosphate by FFA involves adsorption onto fly ash, which is an extensive process on the fly ash surface. This pH-dependent phosphate adsorption indicates that the surface complexation is dominant in the adsorption process (Li et al. 2016). Initially the phosphate ions are transported from the bulk solution to the external liquid film as indicated in the liquid film diffusion model. These ions then migrate into the macro and micro pores of the composite at a higher rate.

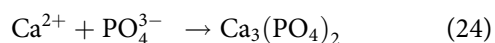
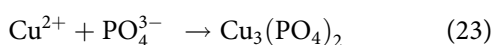
Once the phosphate ions are in the composite, they can make chemical bonds with free Cu^{2+} and Ca^{2+} ions to form $\text{Cu}_3(\text{PO}_4)_2$ and $\text{Ca}_3(\text{PO}_4)_2$ and precipitate (Equations (23) and (24)) (Luengo et al. 2006). These precipitates render the composite surface homogeneous and to possess the same adsorption energies. Thereafter the adsorption takes place giving rise to a monolayer sorption as suggested by the Langmuir model. With time, the phosphate concentration decreases due to adsorption and then it follows multi-layer adsorption.

The optimum pH for adsorption onto the composite FFA was recorded in the acidic range pH 3–7 within which the metal active sites are protonated because of the high H^+ ion concentration present in the solution. These protonated

Table 5. A comparison of selected parameters from recent studies on phosphate adsorption.

Adsorbent	PO ₄ ³⁻ concentration/ mg L ⁻¹	Equilibrium time	Maximum adsorption	pH	Isotherm model	Kinetic model
Hydrous niobium oxide (Rodrigues and da Silva 2010)	50	5 h	80%	2	Langmuir	Pseudo 2 nd order
Fe(III)-AM-PGMA Cell (Anirudhan and Senan 2011)	50	2 h	97.2 % (20 °C)	6	Sips	Pseudo 1 st order
Chitosan immobilized <i>Scenedesmus</i> (Fierro, del Pilar Sánchez-Saavedra, and Copalcua 2008)	6	12 h	94%	NA	NA	NA
Chitosan beads (Fierro, del Pilar Sánchez-Saavedra, and Copalcua 2008)	6	80 h	60%	NA	NA	NA
Hexadecyldimethylammonium loaded clinoptilolite (Bhardwaj et al. 2014)	340	25 h	85%	7	Langmuir	Pseudo 2 nd order
Diocetadecyldimethylammonium loaded clinoptilolite (Bhardwaj et al. 2014)		12 h	80%	7	Langmuir	Pseudo 2 nd order
Mixed Lanthanum/Aluminum pillared clay (Tian et al. 2009)	10	5 h	3 mgP/g	3–5	Freundlich	Pseudo 1 st order
Aluminum pillared clay (Tian et al. 2009)	10	6 h	1 mgP/g	3–5	Freundlich	Pseudo 1st order
Fe-Mn binary oxide (Zhang et al. 2009)	5	11 h	98%	3–5	Freundlich	Pseudo 2 nd order
Alginate/iron(III) chloride capsules 20 °C (Siwek et al. 2016)	10	48 h	89.5%	4–10	Freundlich	NA
Goethite (Luengo et al. 2006)	5.47 × 10 ⁻⁵ M	300 min	NA	NA	NA	NA
Feldspar-alginate-agar (This study)	5	9.5 h	81%	4–10	Freundlich	Pseudo 2 nd order
Feldspar-Flyash-Alginate (This study)	5	5.5 h	82%	3–7	Freundlich	Pseudo 2 nd order

sites become Lewis acids accepting electrons. Consequently, the phosphate ions become Lewis base acting as electron donors (Li et al. 2016). This Lewis acid-base interaction enhances the phosphate removal. The higher phosphate removal is due to the presence of CaCO₃ in the fly ash (Wang and Wu 2006). The phosphate adsorption following surface precipitation is favored by the alkaline pH of the solution.



Significance of the study

The outcome of this study was compared with those from other studies on removal of phosphates by adsorption in Table 5. All the studies indicate a long time period required to reach equilibrium, 5.0 h being the minimum. Of these, hydrous niobium oxide adsorbed 80% in 5.0 h, with a high initial concentration of 50 mg L⁻¹ and an acidic pH of 2 (Rodrigues and da Silva 2010). The mixed Lanthanum/Aluminium pillared clay adsorbed 3 mg of phosphorus from an initial concentration of 10 mg L⁻¹ (Tian et al. 2009) while goethite also required 5 h for

adsorption (Luengo et al. 2006); however, other details are not available. The isotherm models were either Langmuir or Freundlich and most studies followed the pseudo 2nd order kinetic model (Table 5). In this study, we report 80% adsorption of phosphate onto FAA and FFA composites from a realistic initial phosphate concentration of 5 mg L⁻¹ at an equilibrium time of 9.5 h and 5.5 h, respectively, which compares well with that ranging from 11 to 80 h from the rest of the studies (Table 5).

Between the two composite materials, FAA and FFA, the adsorption percentages were almost the same (80–82%); however, 9.5 h equilibrium time was reported for FAA while it was 5.5 h for FFA. The FAA composite adsorbed phosphate ions in the pH range of pH 4–10 and FFA in the range of pH 3–7. Even though the FAA composite adsorbed phosphate in a wide pH range, FFA composite, which consumes less time, is more suitable for the adsorption of phosphates from wastewater.

Concluding remarks

The composite, Feldspar-Alginate-Agar cross-linked with Ca²⁺ and Fe³⁺ and Feldspar-Fly ash-

Alginate crosslinked with Cu^{2+} can be successfully used to adsorb phosphate from aqueous solutions and equilibrium was reached after 9.5 h and 5.5 h, respectively, with around 80% phosphate adsorption. The optimum pH range was 4–10 for FAA composite, whereas pH 3–7 is suitable for FFA composite. The kinetics of the adsorption process is explained by pseudo 2nd order kinetic model. Isotherm studies suggest the operation of diffusion models at different stages of adsorption: intraparticle and liquid film diffusion models, Langmuir, Freundlich, Langmuir–Freundlich combined model, and Dubinin–Radushkevich isotherm models. The FT-IR spectrum supports the presence of hydroxyl, carbonyl, carboxylate, alkane groups, and ether groups in the composite. The components of this biopolymer-based composite are commonly available and inexpensive. It is easily synthesized and can potentially be scaled up for phosphate removal from aqueous systems. Further studies to recover phosphates from the phosphate-loaded adsorbent can be used for the provision of plant nutrition and to complete the phosphate cycle.

Acknowledgments

The authors express their gratitude to Ms. Shirani Perera and Mr. R. B. Hapukotuwa of the National Institute of Fundamental Studies, Sri Lanka for their support during the research. The financial support under grant no. NRC 15-022 from the National Research Council of Sri Lanka is gratefully acknowledged.

Disclosure statement

No potential conflict of interest was reported by the authors.

List of abbreviations

C_i	Initial phosphate concentrations (mg L^{-1})
C_f	Final phosphate concentrations (mg L^{-1})
FAA	Feldspar-Agar-Alginate composite
FFA	Feldspar-Fly ash-Alginate composite
q	Adsorption capacity (mg g^{-1})
V	Volume of the phosphate solution (mL)
M	Mass of the adsorbent (g)
q_t	Amount of solute adsorbed on the adsorbent at time t (mg g^{-1})

q_e	Amount of solute adsorbed on the adsorbent at equilibrium (mg g^{-1})
k_1	Pseudo 1 st order constants (min^{-1})
k_2	Pseudo 2 nd order constants ($\text{g mg}^{-1} \text{min}^{-1}$)
k_i	Intra-particle diffusion constant ($\text{mg g}^{-1} \text{min}^{-0.5}$)
R^l	Liquid film diffusion constant (min^{-1})
D_e^l	Effective liquid film diffusion coefficient ($\text{cm}^2 \text{min}^{-1}$)
r_0	Radius of the adsorbent particle (cm)
Δr_0	Thickness of the liquid film (cm)
k^l	Adsorption equilibrium constant
q_0	Maximum adsorption capacity (mg g^{-1})
k_L	Langmuir constant (L mg^{-1})
R_L	Adsorption intensity
k_F	Freundlich constant
n	Surface heterogeneity
K_{LF}	Langmuir-Freundlich isotherm constant (L mg^{-1})
C_s	Saturation concentration of phosphate (mg L^{-1})
R	Universal gas constant ($8.314 \text{ J K}^{-1} \text{mol}^{-1}$)
T	Absolute temperature (K)
E	Mean free energy per molecule of adsorbent (kJ mol^{-1})
β	Dubinin–Radushkevich constant ($\text{mol}^2 \text{J}^{-2}$)
R^2	regression coefficient

ORCID

Rasika E. A. Dissanayake  <http://orcid.org/0000-0001-7535-6552>

Sithy S. Iqbal  <http://orcid.org/0000-0003-2706-279X>

Mohamed C. M. Iqbal  <http://orcid.org/0000-0002-4862-5099>

References

- Anirudhan, T. S., and P. Senan. 2011. Adsorption of phosphate ions from water using a novel cellulose-based adsorbent. *Chemistry and Ecology* 27 (2):147–64. doi: [10.1080/02757540.2010.547487](https://doi.org/10.1080/02757540.2010.547487).
- Baral, S. S., N. Das, G. Roy Chaudhury, and S. N. Das. 2009. A preliminary study on the adsorptive removal of Cr(VI) using seaweed, *Hydrilla verticillata*. *Journal of Hazardous Materials* 171 (1-3):358–69. doi: [10.1016/j.jhazmat.2009.06.011](https://doi.org/10.1016/j.jhazmat.2009.06.011).
- Bhardwaj, D., P. Sharma, M. Sharma, and R. Tomar. 2014. Removal and slow release studies of phosphate on surfactant loaded hydrothermally synthesized silicate nanoparticles. *Journal of the Taiwan Institute of Chemical Engineers* 45 (5):2649–58. doi: [10.1016/j.jtice.2014.07.010](https://doi.org/10.1016/j.jtice.2014.07.010).
- Blanchard, G., M. Maunaye, and G. Martin. 1984. Removal of heavy metals from waters by means of natural zeolites. *Water Research* 18 (12):1501–7. doi: [10.1016/0043-1354\(84\)90124-6](https://doi.org/10.1016/0043-1354(84)90124-6).
- Caravelli, A. H., E. M. Contreras, and N. E. Zaritzky. 2010. Phosphorous removal in batch systems using ferric

- chloride in the presence of activated sludges. *Journal of Hazardous Materials* 177 (1-3):199–208. doi: [10.1016/j.jhazmat.2009.12.018](https://doi.org/10.1016/j.jhazmat.2009.12.018).
- Chan, L. W., Y. Jin, and P. W. S. Heng. 2002. Cross-linking mechanisms of calcium and zinc in production of alginate microspheres. *International Journal of Pharmaceutics* 242 (1-2):255–8. doi: [10.1016/S0378-5173\(02\)00169-2](https://doi.org/10.1016/S0378-5173(02)00169-2).
- Chathuranga, P. D., N. Priyantha, S. S. Iqbal, and M. M. Iqbal. 2013. Biosorption of Cr (III) and Cr (VI) species from aqueous solution by *Cabomba caroliniana*: Kinetic and equilibrium study. *Environmental Earth Sciences* 70 (2):661–71.
- Daniel, T. C., A. N. Sharpley, and J. L. Lemunyon. 1998. Agricultural phosphorus and eutrophication: A symposium overview. *Journal of Environmental Quality* 27 (2): 251–7. doi: [10.2134/jeq1998.00472425002700020002x](https://doi.org/10.2134/jeq1998.00472425002700020002x).
- Das, J., B. S. Patra, N. Baliarsingh, and K. M. Parida. 2006. Adsorption of phosphate by layered double hydroxides in aqueous solutions. *Applied Clay Science* 32 (3-4):252–60. doi: [10.1016/j.clay.2006.02.005](https://doi.org/10.1016/j.clay.2006.02.005).
- Dissanayake, D. M. R. E. A., W. M. K. E. H. Wijesinghe, S. S. Iqbal, N. Priyantha, and M. C. M. Iqbal. 2016. Fuchsin biosorption using *Asplenium nidus* biosorbent—A mechanism using kinetic and isotherm data. *RSC Advances* 6 (101):98682–92. doi: [10.1039/C6RA19011A](https://doi.org/10.1039/C6RA19011A).
- Du, W., Y. Li, X. Xu, Y. Shang, B. Gao, and Q. Yue. 2019. Selective removal of phosphate by dual Zr and La hydroxide/cellulose-based bio-composites. *Journal of Colloid and Interface Science* 533:692–9. doi: [10.1016/j.jcis.2018.09.002](https://doi.org/10.1016/j.jcis.2018.09.002).
- Dubin, M. M., and L. V. Radushkevich. 1947. Equation of the characteristic curve of activated charcoal. *Chemisches Zentralblatt* 1 (1):875.
- Duckworth, M., and W. Yaphe. 1971. The structure of agar: Part I. Fractionation of a complex mixture of polysaccharides. *Carbohydrate Research* 16 (1):189–97. doi: [10.1016/S0008-6215\(00\)86113-3](https://doi.org/10.1016/S0008-6215(00)86113-3).
- Fierro, S., M. del Pilar Sánchez-Saavedra, and C. Copalca. 2008. Nitrate and phosphate removal by chitosan immobilized *Scenedesmus*. *Bioresource Technology* 99 (5): 1274–9. doi: [10.1016/j.biortech.2007.02.043](https://doi.org/10.1016/j.biortech.2007.02.043).
- Freundlich, H. M. F. 1906. Over the adsorption in solution. *Journal of Physical Chemistry*. 57 (385471):1100–7.
- Gilbert, N. 2009. Environment: The disappearing nutrient. *Nature News* 461 (7265):716–8. doi: [10.1038/461716a](https://doi.org/10.1038/461716a).
- Goscianska, J., M. Ptazkowska-Koniarz, M. Frankowski, M. Franus, R. Panek, and W. Franus. 2018. Removal of phosphate from water by lanthanum-modified zeolites obtained from fly ash. *Journal of Colloid and Interface Science* 513:72–81. doi: [10.1016/j.jcis.2017.11.003](https://doi.org/10.1016/j.jcis.2017.11.003).
- Gu, W., Q. Xie, M. Xing, and D. Wu. 2017. Enhanced adsorption of phosphate onto zinc ferrite by incorporating cerium. *Chemical Engineering Research and Design* 117:706–14. doi: [10.1016/j.cherd.2016.11.026](https://doi.org/10.1016/j.cherd.2016.11.026).
- He, J., Y. Xu, W. Wang, B. Hu, Z. Wang, X. Yang, Y. Wang, and L. Yang. 2020. Ce (III) nanocomposites by partial thermal decomposition of Ce-MOF for effective phosphate adsorption in a wide pH range. *Chemical Engineering Journal* 379:122431. doi: [10.1016/j.cej.2019.122431](https://doi.org/10.1016/j.cej.2019.122431).
- Ho, Y.-S. 2006. Review of second-order models for adsorption systems. *Journal of Hazardous Materials* 136 (3): 681–9. doi: [10.1016/j.jhazmat.2005.12.043](https://doi.org/10.1016/j.jhazmat.2005.12.043).
- Jang, J., and D. S. Lee. 2019. Effective phosphorus removal using chitosan/Ca-organically modified montmorillonite beads in batch and fixed-bed column studies. *Journal of Hazardous Materials* 375:9–18. doi: [10.1016/j.jhazmat.2019.04.070](https://doi.org/10.1016/j.jhazmat.2019.04.070).
- Jeppu, G. P., and T. P. Clement. 2012. A modified Langmuir-Freundlich isotherm model for simulating pH-dependent adsorption effects. *Journal of Contaminant Hydrology* 129:46–53.
- Jiang, H., P. Chen, S. Luo, X. Tu, Q. Cao, and M. Shu. 2013. Synthesis of novel nanocomposite Fe₃O₄/ZrO₂/chitosan and its application for removal of nitrate and phosphate. *Applied Surface Science* 284:942–9. doi: [10.1016/j.apsusc.2013.04.013](https://doi.org/10.1016/j.apsusc.2013.04.013).
- Lagergren, S. K. 1898. About the theory of so-called adsorption of soluble substances. *Kungliga Svenska Vetenskapsakademiens Handlingar* 24:1–39.
- Lahaye, M., and C. Rochas. 1991a. Chemical structure and physico-chemical properties of agar. In *International Workshop on Gelidium. Developments in Hydrobiology*, ed. J. A. Juanes, B. Santelices, and J. L. McLachlan, vol 68. Dordrecht: Springer. doi: [10.1007/978-94-011-3610-5_13](https://doi.org/10.1007/978-94-011-3610-5_13).
- Lahaye, M., and C. Rochas. 1991b. Chemical structure and physico-chemical properties of agar. *Hydrobiologia* 221 (1):137–48. doi: [10.1007/BF00028370](https://doi.org/10.1007/BF00028370).
- Langmuir, I. 1918. The adsorption of gases on plane surfaces of glass, mica and platinum. *Journal of the American Chemical Society* 40 (9):1361–403. doi: [10.1021/ja02242a004](https://doi.org/10.1021/ja02242a004).
- Lee, K. Y., and D. J. Mooney. 2012. Alginate: Properties and biomedical applications. *Progress in Polymer Science* 37 (1):106–26. doi: [10.1016/j.progpolymsci.2011.06.003](https://doi.org/10.1016/j.progpolymsci.2011.06.003).
- Li, M., J. Liu, Y. Xu, and G. Qian. 2016. Phosphate adsorption on metal oxides and metal hydroxides: A comparative review. *Environmental Reviews* 24 (3):319–32. doi: [10.1139/er-2015-0080](https://doi.org/10.1139/er-2015-0080).
- Li, Y., C. Liu, Z. Luan, X. Peng, C. Zhu, Z. Chen, Z. Zhang, J. Fan, and Z. Jia. 2006. Phosphate removal from aqueous solutions using raw and activated red mud and fly ash. *Journal of Hazardous Materials* 137 (1):374–83. doi: [10.1016/j.jhazmat.2006.02.011](https://doi.org/10.1016/j.jhazmat.2006.02.011).
- Lin, J., Y. Zhan, H. Wang, M. Chu, C. Wang, Y. He, and X. Wang. 2017. Effect of calcium ion on phosphate adsorption onto hydrous zirconium oxide. *Chemical Engineering Journal* 309:118–29. doi: [10.1016/j.cej.2016.10.001](https://doi.org/10.1016/j.cej.2016.10.001).
- Liu, B., Y. Yu, Q. Han, S. Lou, L. Zhang, and W. Zhang. 2020. Fast and efficient phosphate removal on lanthanum-chitosan composite synthesized by controlling the amount of cross-linking agent. *International Journal of Biological Macromolecules* 157:247–58. doi: [10.1016/j.ijbiomac.2020.04.159](https://doi.org/10.1016/j.ijbiomac.2020.04.159).

- Liu, H., W. Guo, Z. Liu, X. Li, and R. Wang. 2016. Effective adsorption of phosphate from aqueous solution by La-based metal-organic frameworks. *RSC Advances* 6 (107): 105282–7. doi: [10.1039/C6RA24568D](https://doi.org/10.1039/C6RA24568D).
- Lu, Y., and E. Wilkins. 1996. Heavy metal removal by caustic-treated yeast immobilized in alginate. *Journal of Hazardous Materials* 49 (2-3):165–79. doi: [10.1016/0304-3894\(96\)01754-2](https://doi.org/10.1016/0304-3894(96)01754-2).
- Luengo, C., M. Brigante, J. Antelo, and M. Avena. 2006. Kinetics of phosphate adsorption on goethite: Comparing batch adsorption and ATR-IR measurements. *Journal of Colloid and Interface Science* 300 (2):511–8. doi: [10.1016/j.jcis.2006.04.015](https://doi.org/10.1016/j.jcis.2006.04.015).
- Luo, X., X. Wang, S. Bao, X. Liu, W. Zhang, and T. Fang. 2016. Adsorption of phosphate in water using one-step synthesized zirconium-loaded reduced graphene oxide. *Scientific Reports* 6:39108. doi: [10.1038/srep39108](https://doi.org/10.1038/srep39108).
- Mao, Y., and Q. Yue. 2016. Kinetic modeling of phosphate adsorption by preformed and in situ formed hydrous ferric oxides at circumneutral pH. *Scientific Reports* 6 (1): 35292. doi: [10.1038/srep35292](https://doi.org/10.1038/srep35292).
- Murphy, J., and J. P. Riley. 1962. A modified single solution method for the determination of phosphate in natural waters. *Analytica Chimica Acta* 27:31–6. doi: [10.1016/S0003-2670\(00\)88444-5](https://doi.org/10.1016/S0003-2670(00)88444-5).
- Oehmen, A., P. C. Lemos, G. Carvalho, Z. Yuan, J. Keller, L. L. Blackall, and M. A. M. Reis. 2007. Advances in enhanced biological phosphorus removal: From micro to macro scale. *Water Research* 41 (11):2271–300. doi: [10.1016/j.watres.2007.02.030](https://doi.org/10.1016/j.watres.2007.02.030).
- Ogata, F., E. Ueta, M. Toda, M. Otani, and N. Kawasaki. 2017. Adsorption of phosphate ions from an aqueous solution by calcined nickel-cobalt binary hydroxide. *Water Science and Technology* 75 (1-2):94–105. doi: [10.2166/wst.2016.492](https://doi.org/10.2166/wst.2016.492).
- Pan, M., X. Lin, J. Xie, and X. Huang. 2017. Kinetic, equilibrium and thermodynamic studies for phosphate adsorption on aluminum hydroxide modified palygorskite nano-composites. *RSC Advances* 7 (8):4492–500. doi: [10.1039/C6RA26802A](https://doi.org/10.1039/C6RA26802A).
- Parsons, I. 2012. *Feldspars and their reactions*. Vol. 421. Dordrecht, The Netherlands: Kluwer Academic Publishers.
- Pavia, D. L., G. M. Lampman, G. S. Kriz, and J. A. Vyvyan. 2008. *Introduction to spectroscopy*. United States of America: Cengage Learning.
- Qiu, H., L. Lv, B-c Pan, Q-j Zhang, W-m Zhang, and Q-x Zhang. 2009. Critical review in adsorption kinetic models. *Journal of Zhejiang University-Science A* 10 (5):716–24. doi: [10.1631/jzus.A0820524](https://doi.org/10.1631/jzus.A0820524).
- Rodrigues, L. A., and M. L. C. P. da Silva. 2010. Adsorption kinetic, thermodynamic and desorption studies of phosphate onto hydrous niobium oxide prepared by reverse microemulsion method. *Adsorption* 16 (3):173–81. doi: [10.1007/s10450-010-9220-7](https://doi.org/10.1007/s10450-010-9220-7).
- Rosemarin, A. 2004. The precarious geopolitics of phosphorous. *Down to Earth* 30:27–34.
- Selim, A. Q., L. Sellaoui, and M. Mobarak. 2019. Statistical physics modeling of phosphate adsorption onto chemically modified carbonaceous clay. *Journal of Molecular Liquids* 279:94–107. doi: [10.1016/j.molliq.2019.01.100](https://doi.org/10.1016/j.molliq.2019.01.100).
- Silverstein, R. M., and G. C. Bassler. 1962. Spectrometric identification of organic compounds. *Journal of Chemical Education* 39 (11):546. doi: [10.1021/ed039p546](https://doi.org/10.1021/ed039p546).
- Singh, P., S. Kumar Singh, J. Bajpai, A. Kumar Bajpai, and R. B. Shrivastava. 2014. Iron crosslinked alginate as novel nanosorbents for removal of arsenic ions and bacteriological contamination from water. *Journal of Materials Research and Technology* 3 (3):195–202. doi: [10.1016/j.jmrt.2014.03.005](https://doi.org/10.1016/j.jmrt.2014.03.005).
- Siwek, H., A. Bartkowiak, M. Włodarczyk, and K. Sobiecka. 2016. Removal of phosphate from aqueous solution using alginate/iron (III) chloride capsules: A laboratory study. *Water, Air, and Soil Pollution* 227 (11):427. doi: [10.1007/s11270-016-3128-0](https://doi.org/10.1007/s11270-016-3128-0).
- Soares, J. P., J. E. Santos, G. O. Chierice, and E. T. G. Cavaleiro. 2004. Thermal behavior of alginic acid and its sodium salt. *Eclética Química* 29 (2):57–64. doi: [10.1590/S0100-46702004000200009](https://doi.org/10.1590/S0100-46702004000200009).
- Tian, S., P. Jiang, P. Ning, and Y. Su. 2009. Enhanced adsorption removal of phosphate from water by mixed lanthanum/aluminum pillared montmorillonite. *Chemical Engineering Journal* 151 (1-3):141–8. doi: [10.1016/j.cej.2009.02.006](https://doi.org/10.1016/j.cej.2009.02.006).
- Tran, H. N., S.-J. You, and H.-P. Chao. 2016. Thermodynamic parameters of cadmium adsorption onto orange peel calculated from various methods: A comparison study. *Journal of Environmental Chemical Engineering* 4 (3):2671–82. doi: [10.1016/j.jece.2016.05.009](https://doi.org/10.1016/j.jece.2016.05.009).
- Wang, N., J. Feng, J. Chen, J. Wang, and W. Yan. 2017. Adsorption mechanism of phosphate by polyaniline/TiO₂ composite from wastewater. *Chemical Engineering Journal* 316:33–40. doi: [10.1016/j.cej.2017.01.066](https://doi.org/10.1016/j.cej.2017.01.066).
- Wang, S., Y. Boyjoo, A. Choueib, and Z. H. Zhu. 2005. Removal of dyes from aqueous solution using fly ash and red mud. *Water Research* 39 (1):129–38. doi: [10.1016/j.watres.2004.09.011](https://doi.org/10.1016/j.watres.2004.09.011).
- Wang, S., and H. Wu. 2006. Environmental-benign utilisation of fly ash as low-cost adsorbents. *Journal of Hazardous Materials* 136 (3):482–501. doi: [10.1016/j.jhazmat.2006.01.067](https://doi.org/10.1016/j.jhazmat.2006.01.067).
- Wang, W., C. Ma, Y. Zhang, S. Yang, Y. Shao, and X. Wang. 2016. Phosphate adsorption performance of a novel filter substrate made from drinking water treatment residuals. *Journal of Environmental Sciences (China)* 45: 191–9. doi: [10.1016/j.jes.2016.01.010](https://doi.org/10.1016/j.jes.2016.01.010).
- Wang, X., F. Liu, W. Tan, W. Li, X. Feng, and D. L. Sparks. 2013. Characteristics of phosphate adsorption-desorption onto ferrihydrite: Comparison with well-crystalline Fe (hydr) oxides. *Soil Science* 178 (1):1–11. doi: [10.1097/SS.0b013e31828683f8](https://doi.org/10.1097/SS.0b013e31828683f8).
- Weber, W. J., and J. C. Morris. 1963. Kinetics of adsorption on carbon from solution. *Journal of the Sanitary Engineering Division* 89 (2):31–60.

- Xiong, W., J. Tong, Z. Yang, G. Zeng, Y. Zhou, D. Wang, P. Song, R. Xu, C. Zhang, and M. Cheng. 2017. Adsorption of phosphate from aqueous solution using iron-zirconium modified activated carbon nanofiber: Performance and mechanism. *Journal of Colloid and Interface Science* 493:17–23. doi: [10.1016/j.jcis.2017.01.024](https://doi.org/10.1016/j.jcis.2017.01.024).
- Yao, Y., B. Gao, M. Inyang, A. R. Zimmerman, X. Cao, P. Pullammanappallil, and L. Yang. 2011. Biochar derived from anaerobically digested sugar beet tailings: Characterization and phosphate removal potential. *Bioresource Technology* 102 (10):6273–8.
- Yazdani, M., N. Mohammad Mahmoodi, M. Arami, and H. Bahrami. 2012. Isotherm, kinetic, and thermodynamic of cationic dye removal from binary system by Feldspar. *Separation Science and Technology* 47 (11):1660–72. doi: [10.1080/01496395.2011.654169](https://doi.org/10.1080/01496395.2011.654169).
- Ye, J., X. Cong, P. Zhang, E. Hoffmann, G. Zeng, Y. Liu, W. Fang, Y. Wu, and H. Zhang. 2015. Interaction between phosphate and acid-activated neutralized red mud during adsorption process. *Applied Surface Science* 356:128–34. doi: [10.1016/j.apsusc.2015.08.053](https://doi.org/10.1016/j.apsusc.2015.08.053).
- Yoon, H.-S., K. W. Chung, C.-J. Kim, J.-H. Kim, H.-S. Lee, S.-J. Kim, S.-I. Lee, S.-J. Yoo, and B.-C. Lim. 2018. Characteristics of phosphate adsorption on ferric hydroxide synthesized from a $\text{Fe}_2(\text{SO}_4)_3$ aqueous solution discharged from a hydrometallurgical process. *Korean Journal of Chemical Engineering* 35 (2):470–8. doi: [10.1007/s11814-017-0287-7](https://doi.org/10.1007/s11814-017-0287-7).
- Zhang, G., H. Liu, R. Liu, and J. Qu. 2009. Removal of phosphate from water by a Fe-Mn binary oxide adsorbent. *Journal of Colloid and Interface Science* 335 (2): 168–74. doi: [10.1016/j.jcis.2009.03.019](https://doi.org/10.1016/j.jcis.2009.03.019).
- Zhang, Y.-h., F.-q. Liu, C.-q. Zhu, X.-p. Zhang, M.-m. Wei, F.-h. Wang, C. Ling, and A.-m. Li. 2017. Multifold enhanced synergistic removal of nickel and phosphate by a (N,Fe)-dual-functional bio-sorbent: Mechanism and application. *Journal of Hazardous Materials* 329:290–8. doi: [10.1016/j.jhazmat.2017.01.054](https://doi.org/10.1016/j.jhazmat.2017.01.054).
- Zhao, T., and T. Feng. 2016. Application of modified chitosan microspheres for nitrate and phosphate adsorption from aqueous solution. *RSC Advances* 6 (93):90878–86. doi: [10.1039/C6RA17474D](https://doi.org/10.1039/C6RA17474D).